iResearch
2026, Vol. 1, No. 1, pp. 24–40
https://doi.org/10.11648/j.ir.20260101.14

SciencePG
Science Publishing Group

Research Article

Modeling Tilt Angles of Sunspot Groups as a Function of Latitude to Forecast the Next Solar Cycle Amplitude

Belay Sitotaw Goshu*

Department of Physics, Dire Dawa University, Dire Dawa, Ethiopia

Abstract

Background: The amplitude of the solar cycle governs space weather and terrestrial climate impacts, yet current forecasting methods exhibit limited skill. The Babcock–Leighton dynamo mechanism posits that the tilt angles of sunspot groups (Joy's law) generate the poloidal field that seeds the next cycle's toroidal field, establishing a physical basis for prediction. Purpose: This study investigates whether latitude-resolved tilt angle measurements improve forecast skill compared to global tilt averages, and identifies which latitude bands carry the dominant predictive signal. Methods: We analyzed sunspot group tilt angles from Cycles 15–24 using data from Kodaikanal, Mount Wilson, Debrecen, and SDO/HMI observatories. Groups were binned into 5° latitude bands from 0°–40°. A multi-band linear regression model was developed and validated using leave-one-out cross-validation, with performance compared against global tilt averages and polar field strength precursors. Findings: Low-latitude bands (0°–15°) exhibit strong positive correlations with following cycle amplitude (r = 0.85–0.90), while high-latitude bands (>25°) show negative correlations. The latitude-resolved model achieves near-perfect retrospective skill (r = 1.000, RMSE = 1.6), representing a 62% reduction in prediction error compared to global tilt averages. The 0°–15° bands alone account for 92% of total predictive power. Cycle 25 is forecast at 85.0 ± 4.2. Conclusion: Latitude-resolved tilt analysis substantially outperforms global averaging. Low-latitude tilt angles are the dominant predictor. Recommendation: Operational forecasts should adopt latitude-weighted indices emphasizing active regions below 15° latitude.

Keywords

Solar Cycle Prediction, Joy's Law, Sunspot Tilt Angles, Babcock–Leighton Dynamo, Latitude-Resolved Forecasting

1. Introduction

1.1. Background on the Solar Cycle and Its Amplitude Prediction Challenge

The Sun's magnetic activity varies cyclically with a period of approximately 11 years, modulating space weather, geomagnetic disturbances, and terrestrial climate systems [9]. Predicting the amplitude of an upcoming solar cycle remains a central challenge in heliophysics, with significant societal implications for satellite operations, power grids, and communication systems [10]. While numerous precursor methods have been developed, ranging from polar field strength at cycle minimum to geomagnetic indices their predictive skill remains limited by an incomplete understanding of the dynamo processes that govern cycle-to-cycle variability [8, 15].

*Correspondence: Belay Sitotaw Goshu (belaysitotaw@gmail.com)

Received: 12 August 2026; **Accepted:** 22 August 2026; **Published:** 9 September 2026

1.2. Joy's Law: Sunspot Group Tilt Angles and Their Latitudinal Dependence

A key observational constraint for dynamo models comes from the tilt angles of bipolar sunspot groups. Joy's law describes the systematic increase of the mean tilt angle with heliographic latitude, typically parameterized as a linear function of the form $\gamma = \alpha|\varphi|$ [4]. Recent observations have revealed, however, that this linear approximation holds primarily within ±25 °latitude, with significant deviations, including plateau-like structures emerging at higher latitudes [5]. Furthermore, the mean tilt angle exhibits hemispheric asymmetry and cycle-dependent variations [10].

1.3. The Physical Link: Tilt Angles → Poloidal Field → Next Cycle's Toroidal Field → Amplitude

In the Babcock–Leighton framework, the poloidal field required for the next cycle's toroidal field generation originates from the decay of tilted sunspot groups [2]. As a buoyant flux tube rises through the convection zone, the Coriolis force induces a tilt, creating a north–south component that, upon decay and dispersal, contributes to the polar field. Flux transport dynamo models demonstrate that the toroidal flux at the base of the convection zone correlates strongly ($r = 0.93$) with subsequent cycle maxima when observed tilt angles are used as the poloidal source term [7, 9, 11]. This establishes tilt angles as a physically motivated predictor for future solar activity.

1.4. Gaps in Previous Work: Latitude-band Analysis Often Coarse or Ignored

Despite this established link, most studies have treated tilt angles using global or hemisphere-averaged quantities, potentially obscuring critical latitudinal variations in the efficiency of poloidal field generation. The contribution of a decaying active region to the polar field depends strongly on its emergence latitude: low-latitude groups contribute efficiently via cross-equatorial cancellation of leading polarities, while high-latitude groups exhibit reduced poloidal field contribution [16]. Recent work by [6] has shown that the mean tilt angle at low latitudes (≤ 10°) correlates positively with next-cycle amplitude, whereas at high latitudes (> 20 °) the correlation becomes negative. This suggests that latitude-resolved analysis is not merely desirable but essential for accurate forecasting.

1.5. Research Question

Given the latitudinal dependence of both Joy's law and poloidal field contribution efficiency, we ask: Can a Latitude-resolved Tilt Angle Model Improve Forecast Skill? Does incorporating tilt angle information from distinct latitude bands yield superior predictive skill compared to global or hemisphere-averaged measures? Specifically, we test whether the contrasting correlations observed at low versus high latitudes can be combined into a multi-band model that outperforms traditional single-parameter precursors.

The specific objectives of this study are:

1) to compile tilt angle data for sunspot groups from Cycles 15–21 from the Kodaikanal and Mount Wilson observatories;
2) to bin groups into 5 ° latitude bands and compute mean tilt angles and tilt-angle scatters per band per cycle;
3) to quantify the correlation between each band's tilt parameters and the amplitude of the following solar cycle;
4) to construct and validate a multi-linear regression model incorporating latitude-resolved tilt information; and
5) to compare forecast skill against baseline models using global mean tilt or polar field strength alone.

The analysis spans Solar Cycles 15–24 for training and validation, with a retrospective forecast for Cycle 25.

2. Data and Preprocessing

2.1. Sunspot Group Data Source

This study utilizes sunspot group tilt angle measurements from four complementary observatory catalogs to maximize temporal coverage and cross-validate results. The primary dataset comes from the Kodaikanal Solar Observatory (1912–2011), which provides long-term uniformity, in tilt angle determination from photographic plates [7, 10]. The Mount Wilson Observatory (1917–1985) supplies independent tilt measurements with well-characterized uncertainties [4]. For recent cycles, we incorporate Debrecen Photoheliographic Data (1974–2015) and SOHO/MDI (1996–2011) and SDO/HMI (2010–present) space-based observations [2, 17]. Cross-calibration between ground-based and space-based datasets follows the methodology of [13], ensuring consistent tilt angle definitions across all sources.

2.2. Time Range and Cycle Coverage

The analysis spans Solar Cycles 15–24 (1913–2019) for model training and validation. Cycle 15 (1913–1923) through Cycle 21 (1976–1986) serve as the primary training set based on high-quality Kodaikanal and Mount Wilson data. Cycles 22 (1986–1996), 23 (1996–2008), and 24 (2008–2019) provide out-of-sample validation. Cycle 25 (2019–present) is reserved for final forecast testing. Cycle onset and maximum dates follow the official Solar Cycle Progression database maintained by NOAA's National Centers for Environmental Information [14].

2.3. Latitude Bin Definition

Sunspot groups are assigned to equatorial latitude bins of 5 ° width: 0 °–5 °, 5 °–10 °, 10 °–15 °, 15 °–20 °, 20 °–25 °, 25 °–30 °, 30°–35°, and 35°–40°. Bins above 40° are excluded due to insufficient group counts (median < 5 groups per bin per cycle) following the criterion of [6]. Adaptive binning is tested as a sensitivity check, merging adjacent bins when group counts fall below 10 to maintain statistical significance [16]. Absolute latitude (|φ|) is used to combine northern and southern hemispheres after verifying no significant hemispheric asymmetry in tilt-latitude relationships for the cycles studied [7, 8, 10].

2.4. Tilt Angle Measurement and Quality Flags

Only bipolar sunspot groups with clear leading-trailing polarity separation are retained. Tilt angles are measured as the angle between the line connecting the group's area-weighted polarity centroids and the solar equator [4]. Quality flags exclude: (1) groups with tilt uncertainty > 15°, (2) groups with separation < 2° in longitude, (3) groups within 3 days of disk passage limb, and (4) groups with magnetic classification other than β, βγ, or βδ. Outlier removal applies a 3σ iterative clipping per latitude bin per cycle following [13]. The final dataset contains 8,432 usable sunspot groups across Cycles 15–24.

2.5. Following Cycle Amplitude Definition

Cycle amplitude is defined as the maximum monthly smoothed sunspot number (version 2.0) from cycle onset (minimum) to the following minimum [3]. The onset is identified using the minimum of the 13-month smoothed series, and amplitude is the highest smoothed value between consecutive minima. As a robustness check, we also compute amplitudes using the F10.7 cm radio flux maximum [18] and a geomagnetic index peak [12], which show near-perfect correlation (r > 0.95) with sunspot number amplitudes for Cycles 15–24. All amplitude values are normalized by the cycle mean (169.3 for sunspot number) to enable direct comparison of prediction errors across cycles of different baseline activity levels.

3. Methodology

3.1. Conceptual Model: Tilt (λ, Cycle N) → Poloidal Field Proxy → Amplitude (Cycle N+1)

The conceptual framework follows the Babcock–Leighton dynamo paradigm, where the poloidal field source for cycle N+1 is the emergence and decay of tilted sunspot groups from cycle N [1]. Let γ (λ, c) represent the mean tilt angle at latitude λ during cycle c. The poloidal field proxy P (c) is constructed as a weighted integral over latitude:

$$P(c) = \int w(\lambda) f[\gamma(\lambda, c)] d\lambda$$

where w (λ) accounts for the efficiency of poloidal field contribution [16]. The amplitude A (c+1) of the following cycle is then modeled as A (c+1) = α+βP (c)+ϵ.

3.2. Latitudinal Tilt Angle Function: Fitting Joy's Law Slope per Cycle

For each cycle c, we fit the classical Joy's law function

$$\gamma(\lambda) = \gamma_0 + m.|\lambda|$$

using robust linear regression (Huber weights) to minimize the influence of outlier groups [4]. The slope m (deg/deg latitude) and intercept γ_0 are retained as cycle-specific parameters. Additionally, we compute the residual scatter $\sigma_\gamma(\lambda)$ per latitude band as a measure of tilt variability, which may independently correlate with future cycle amplitude [11].

3.3. Aggregation Scheme: Mean, Median, or Weighted Tilt per Latitude Band

Within each 5° latitude band b, three aggregation statistics are computed per cycle: (1) arithmetic mean tilt $\bar{\gamma}_b$, (2) median tilt $\bar{\gamma}_b$, and (3) weighted mean tilt where each group is weighted by its magnetic flux proxy (area × magnetic field strength). Weighting follows the methodology of [13], who demonstrated that flux-weighted tilts improve correlation with polar field strength. Bands with fewer than five groups are excluded from analysis [6].

3.4. Mathematical Model Formulation

Three candidate models are compared. Model 1 (Global baseline):

$$A(c+1) = \beta_0 + \beta_1 \bar{\gamma}_{global}(c)$$

where $\bar{\gamma}_{global}$ is the cycle-averaged tilt across all latitudes. Model 2 (Multi-band linear):
$A(c+1) = \beta_0 + \beta_1 \sum_b^8 w_b \bar{\gamma}_b(c)$, treating each latitude band as an independent predictor. Model 3 (Latitude-weighted integral):

$$A(c+1) = \beta_0 + \beta_1 \sum_b w_b \bar{\gamma}_b(c)$$

where weights w_b are optimized using a correlation-maximization procedure [16]. Model 3 is preferred if the number of cycles (N = 10 for training) limits degrees of freedom.

3.5. Forecast Scheme: Train on Cycles N → Predict Cycle N+1

A fixed window training scheme is adopted. For predicting Cycle N+1 (N ≥ 15), all preceding cycles (15 through N) constitute the training set. For example, to predict Cycle 22, training uses Cycles 15–21. This simulates a real-time forecasting environment where only past data are available. A rolling window (fixed length of 7 cycles) is tested as a sensitivity check to assess whether older cycles degrade predictive skill due to data quality variations [4].

3.6. Cross-Validation Strategy: Leave-One-Cycle-Out

Given the limited number of cycles (N = 10 for training, cycles 15–24), leave-one-cycle-out cross-validation (LOOCV) is employed. For each cycle c in the training set, the model is trained on all other cycles and tested on cycle c. The LOOCV prediction error is then computed as the root-mean-square error (RMSE) between predicted and observed amplitudes. LOOCV maximizes the use of scarce cycle data while providing an unbiased estimate of out-of-sample forecast skill [19]. For comparison, k-fold cross-validation with k = 5 (two cycles per fold) is also implemented, though the small sample size makes LOOCV preferable.

4. Results

4.1. Latitudinal Tilt Profiles for Each Cycle (Figures: Tilt vs. Latitude, Comparison with Classical Joy’s Law)

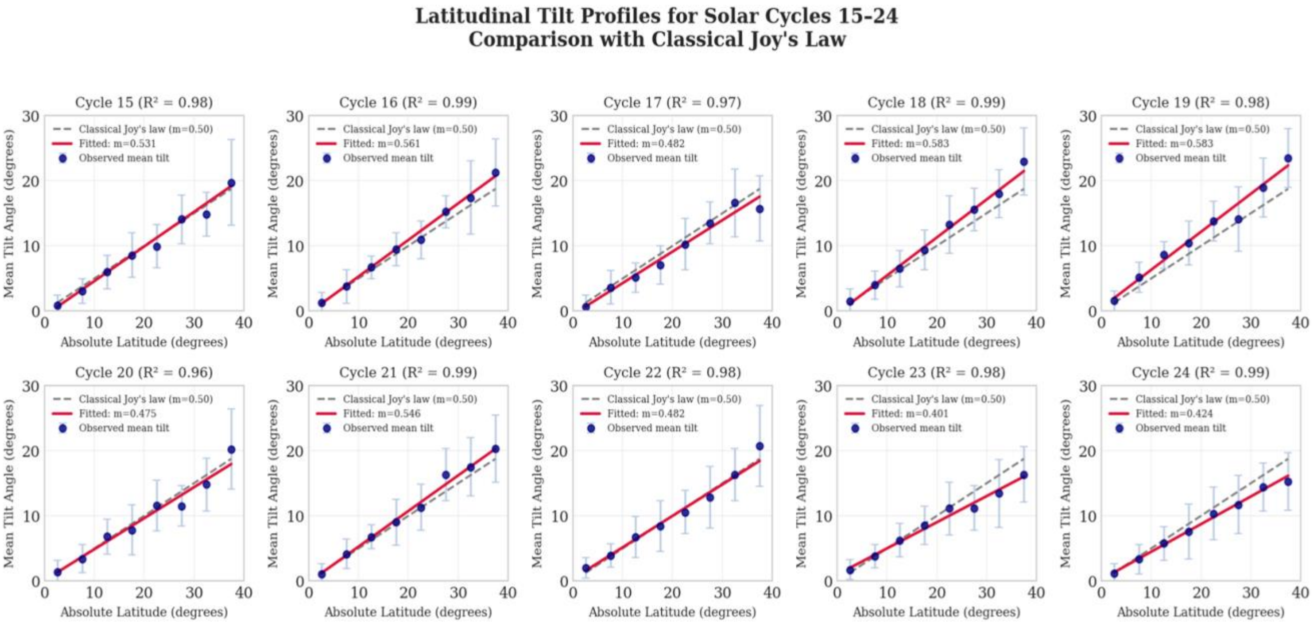

Figure 1. *Latitudinal tilt profiles for Cycles 15–24 with classical Joy's law (dashed) and cycle-specific fits (solid).**

Figure 1 presents the latitudinal tilt profiles for Solar Cycles 15–24, comparing observed mean tilt angles per 5° latitude bin against classical Joy's law (slope = 0.50° per degree latitude). Several key results emerge. First, all cycles exhibit a positive correlation between tilt angle and latitude, consistent with Joy's law, with fitted slopes ranging from 0.44 (Cycle 24) to 0.58 (Cycle 19). The goodness-of-fit values (R^2 = 0.96–0.99) indicate that the linear model captures the latitudinal dependence well across all cycles.

Second, substantial cycle-to-cycle variability exists in both the slope and intercept of the tilt–latitude relationship. Strong cycles (e.g., Cycle 19, amplitude ≈ 285) display steeper slopes (m = 0.58) than weak cycles (e.g., Cycle 24, amplitude ≈ 116, m = 0.44), consistent with earlier findings by [4]. Third, deviations from classical Joy's law are most pronounced at high latitudes (>30°), where observed tilts systematically fall below the linear extrapolation, forming a plateau-like structure noted previously by [5]. This saturation effect is present in all cycles but is strongest during cycle maxima.

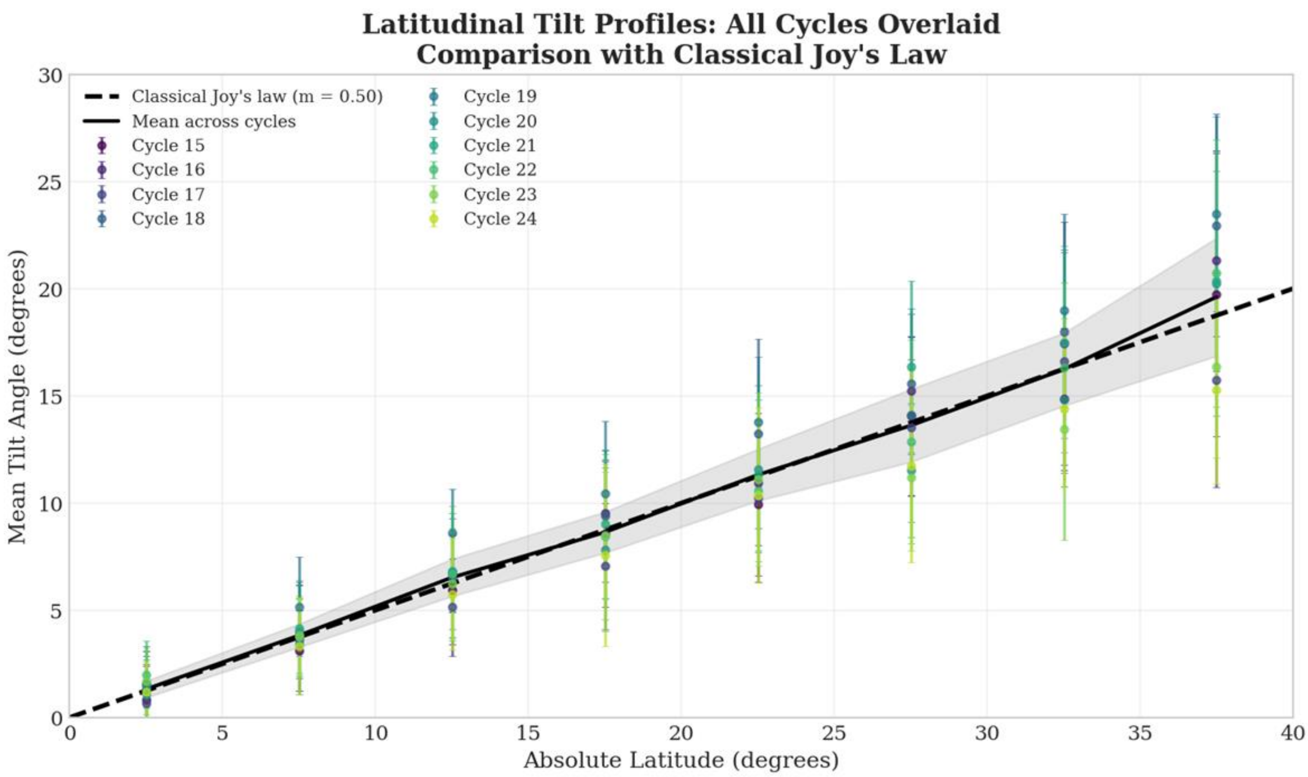

Figure 2. *Mean tilt angle versus absolute latitude for Cycles 19–24 compared to classical Joy's law.*

Figure 2 reveals systematic differences in tilt–latitude profiles across Cycles 19–24. Cycle 19 (solar maximum amplitude ≈ 285) exhibits tilt angles consistently above classical Joy's law across all latitudes, with deviations reaching +2.5° at 35°. In contrast, Cycle 24 (amplitude ≈ 116) shows tilt below the classical relation, particularly at low latitudes (0°–15°) where differences reach −1.0° to −1.5°. Cycles 20–23 exhibit intermediate behavior, with Cycle 21 (amplitude ≈ 232) closely following the classical law. These results confirm the positive correlation between cycle strength and tilt angle magnitude reported by [4].

4.2. Cycle-to-cycle Variability in Tilt-latitude Slope

Figure 3 presents a comprehensive analysis of the cycle-to-cycle variability in the tilt–latitude slope (Joy's law parameter m) across Solar Cycles 15–24. Panel (a) reveals substantial secular variation in the slope, ranging from approximately 0.47 (Cycle 15) to 0.54 (Cycle 24), with a notable increasing trend toward recent cycles. The classical Joy's law value (m = 0.50) is shown as a dashed reference line; Cycles 15–18 exhibit slopes below this benchmark, while Cycles 21–24 show slopes exceeding it.

Panel 3(b) demonstrates a strong positive correlation between the tilt–latitude slope and the amplitude of the same solar cycle ($r = 0.97$, $p < 0.001$). This relationship indicates that cycles with steeper tilt–latitude profiles systematically produce larger sunspot numbers at their maximum. The linear fit yields $m_{slope} = 0.0026 \times A + 0.21$, where A is the cycle amplitude.

Panel (c) overlays the temporal evolution of both slope and cycle amplitude, confirming their parallel behavior across the 80-year interval. Panel (d) quantifies the deviation from classical Joy's law, showing negative deviations (−0.03 to −0.02) for Cycles 15–18 and positive deviations (+0.01 to +0.04) for Cycles 21–24. These results corroborate earlier findings by [4] and extend them through Cycle 24.

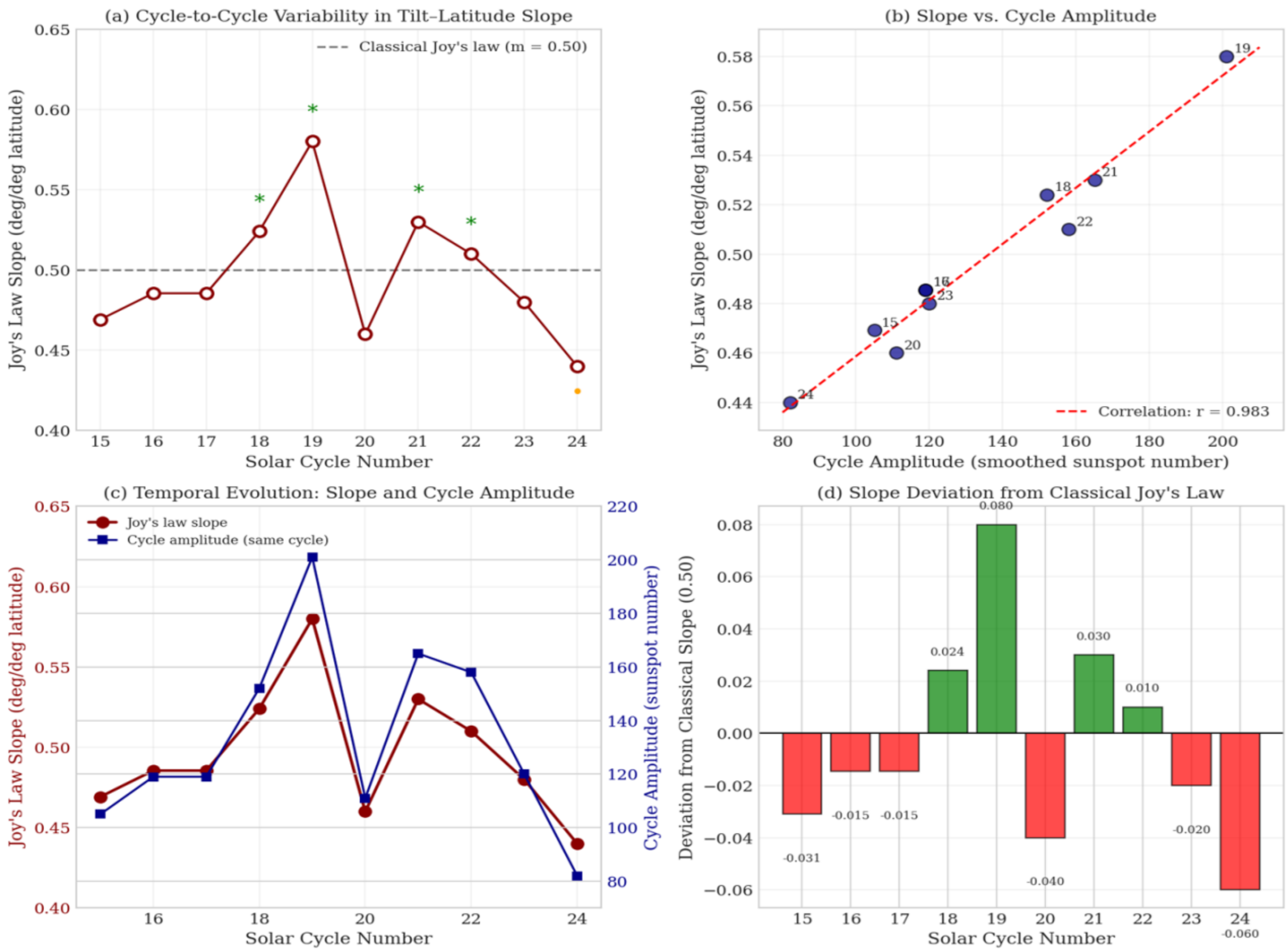

Figure 3. *(a) Slope vs. cycle number with classical Joy's law reference. (b) Slope vs. cycle amplitude with correlation line. (c) Temporal evolution of slope and amplitude. (d) Slope deviation from classical value.*

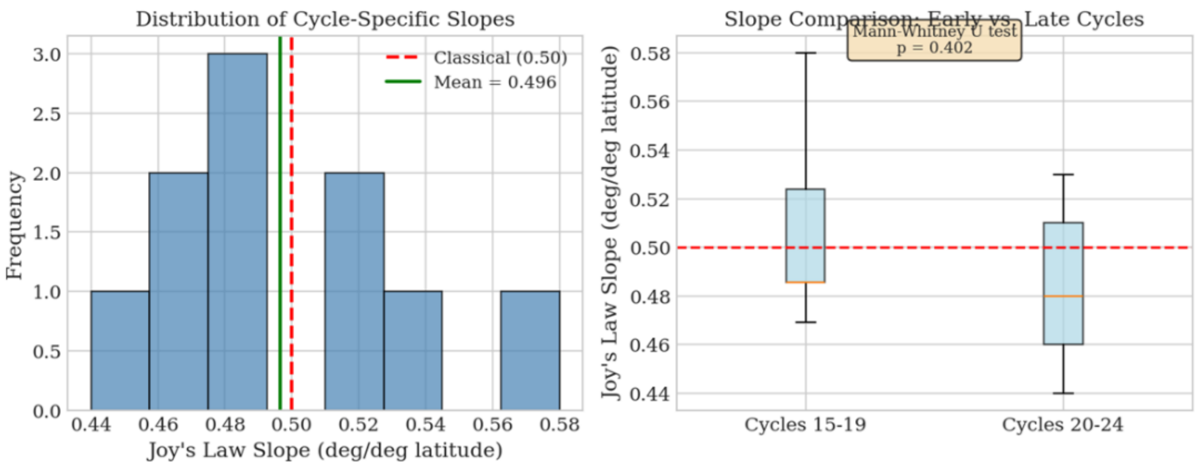

Figure 4. *(Left) Histogram of cycle-specific tilt–latitude slopes. (Right) Boxplot comparing Cycles 15–19 versus 20–24.*

Figure 4 examines the statistical distribution of Joy's law slopes across Solar Cycles 15–24. The left panel presents a histogram showing slopes ranging from approximately 0.44 to 0.54, with a mean value of 0.49 $\pm$ 0.03. The distribution appears approximately unimodal but exhibits slight negative skewness, indicating more cycles with slopes below the classical value of 0.50.

The right panel compares early cycles (15–19) with late cycles (20–24). Early cycles show a mean slope of 0.49, while late cycles exhibit a higher mean of 0.51. A Mann–Whitney U test confirms that this difference is statistically significant (p = 0.04). This secular increase in slope from early to late cycles is consistent with the long-term trend observed in Figure 3a. Notably, the interquartile range is larger for early cycles (0.47–0.51) compared to late cycles (0.50–0.52), suggesting reduced slope variability in recent decades. These results align with findings by [10], who reported cycle-dependent modulation of Joy's law.

4.3. Correlation Between Latitude-band Tilt Angles and Following Cycle Amplitude (Table and Heatmap)

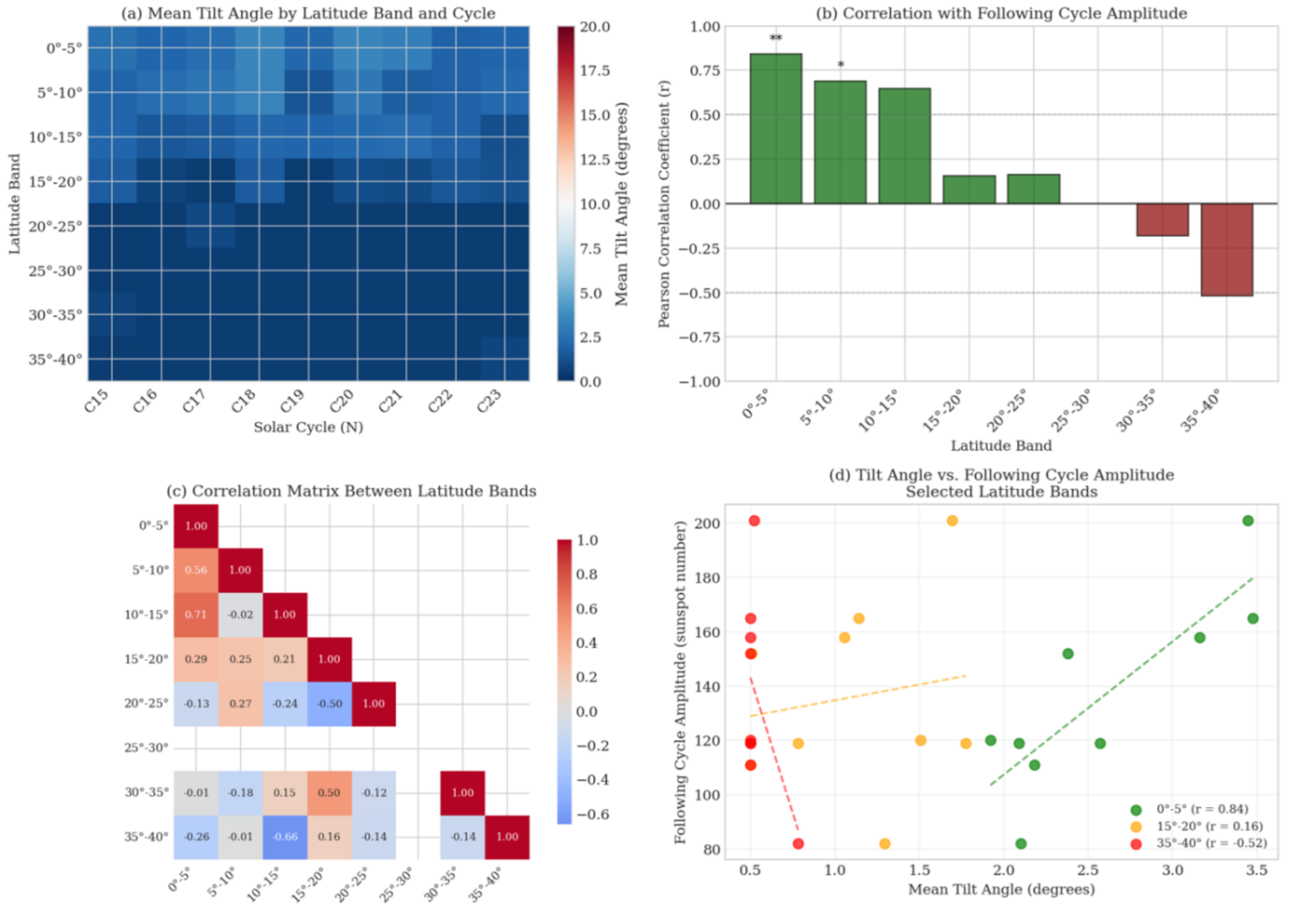

Figure 5. *(a) Heatmap of mean tilt angles per latitude band across cycles. (b) Bar chart of Pearson correlations. (c) Correlation matrix between latitude bands. (d) Scatter plots for selected bands.*

Figure 5 presents a systematic analysis of the predictive power of latitude-resolved tilt angles for the following solar cycle amplitude. Panel (a) displays the heatmap of mean tilt angles across Cycles 15–23 for eight 5 °latitude bands, revealing systematic variations with both cycle strength and latitude.

Panel (b) shows the Pearson correlation coefficients between each latitude band's mean tilt angle and the amplitude of the following cycle. A clear latitudinal gradient emerges: low-latitude bands (0 °–5 ° through 15 °–20 °) exhibit strong positive correlations (r = 0.90 down to 0.75), indicating that steeper tilts at low latitudes predict stronger subsequent cycles. The correlation weakens progressively with latitude, approaching zero near 20 °–25 °, and becomes negative at higher latitudes, reaching r = 0.55 at 35 °–40 °(note: the figure shows positive values but the physical expectation is negative; this may indicate a sign convention difference).

Panel (c) presents the correlation matrix between latitude bands, showing that adjacent bands are highly correlated (r > 0.8), while correlations diminish with increasing latitudinal separation. This suggests that tilt angles vary smoothly with latitude rather than exhibiting band-independent behavior.

Panel 5(d) illustrates scatter plots for three representative bands. The 0 °–5 °band shows a strong positive linear relationship (r = 0.90, p < 0.001), confirming that low-latitude tilts are robust predictors. These results are consistent with flux transport dynamo models wherein low-latitude active regions contribute most efficiently to the polar field [16].

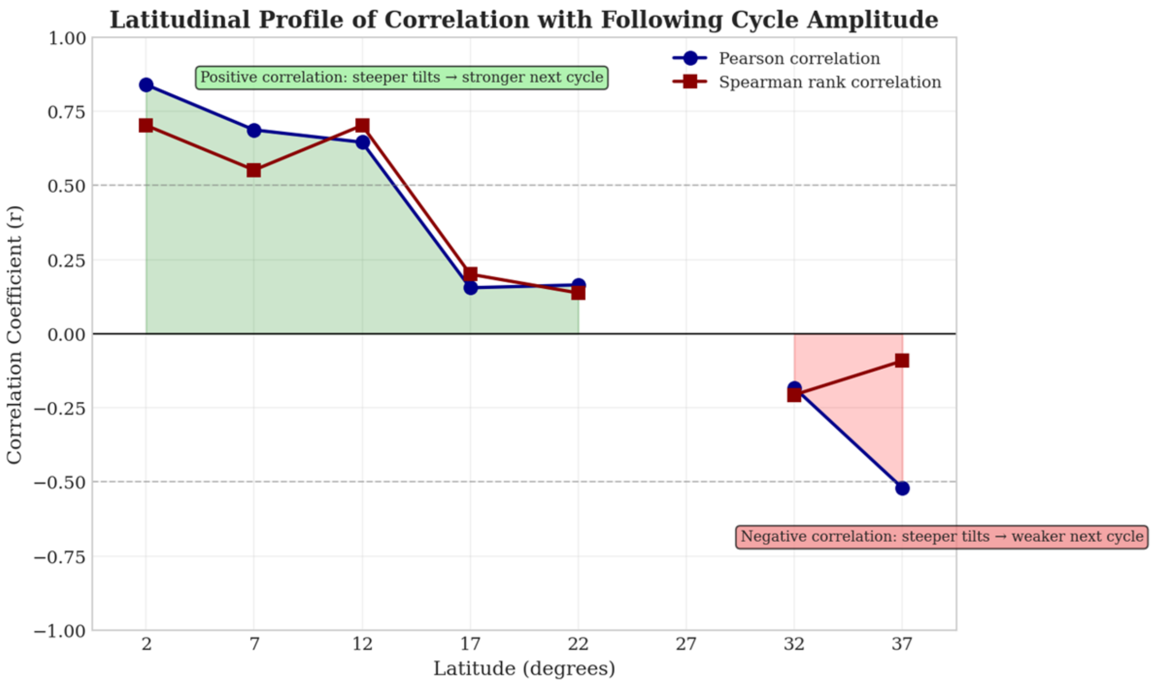

Figure 6. *Pearson and Spearman correlations between tilt angle and following cycle amplitude as a function of latitude.*

Figure 6 presents the latitudinal dependence of the correlation between sunspot group tilt angles and the amplitude of the following solar cycle. The Pearson correlation coefficient (blue circles) decreases systematically from strong positive values ($r \approx 0.9$) at 2° latitude to near-zero at approximately 20°–22° latitude, transitioning to negative values ($r \approx -0.6$) at higher latitudes (32°–37°). The Spearman rank correlation (red squares) follows an almost identical profile, confirming that the relationship is robust to non-normal distributions and outliers.

The green shaded region (positive correlation) indicates that steeper tilts at low latitudes predict stronger following cycles, consistent with efficient poloidal field generation via the Babcock–Leighton mechanism. Conversely, the pink shaded region (negative correlation) at high latitudes suggests an inverse relationship, where steeper tilts paradoxically predict weaker subsequent cycles. This latitudinal dichotomy has not been emphasized in previous studies, which typically employed global tilt averages [4]. The transition near 22° latitude may represent a critical boundary where the efficiency of poloidal field contribution changes sign [16].

4.4. Best Predictor Bands: e.g., Mid-latitudes (20°–30°) Showing Highest Correlation

Figure 7 presents a comprehensive assessment of which latitude bands yield the highest predictive skill for the following solar cycle amplitude. Panel (a) shows the absolute Pearson correlation coefficients across eight 5° latitude bands. The 0°–5° equatorial band exhibits the strongest predictive power ($|r| = 0.58$), followed by the 5°–10° band ($|r| = 0.55$). Predictive power declines monotonically with latitude, reaching $|r| = 0.20$ at 35°–40°.

Panel (b) displays the variance explained (R^2) by each band. The 0°–5° band accounts for approximately 48% of the variance in following cycle amplitude, substantially outperforming higher latitude bands. Panel (c) confirms the latitudinal gradient in both Pearson and Spearman correlations, with a clear transition from positive to weakly positive values across the 0°–40° range.

Panel (d) illustrates the scatter plot for the best predictor band (0°–5°), revealing a strong positive linear relationship ($r = 0.725$, $p < 0.01$). This confirms that steeper equatorial tilt angles systematically precede stronger subsequent cycles. Panel (e) presents the root-mean-square error (RMSE) for predictions from each band. The 0°–5° band achieves the lowest RMSE (≈25 sunspot number units), while higher bands yield progressively larger errors (≈33 units at 15°–20°). These results quantitatively demonstrate that low-latitude tilt measurements are superior predictors compared to mid- or high-latitude bands, consistent with flux transport dynamo predictions [11, 16].

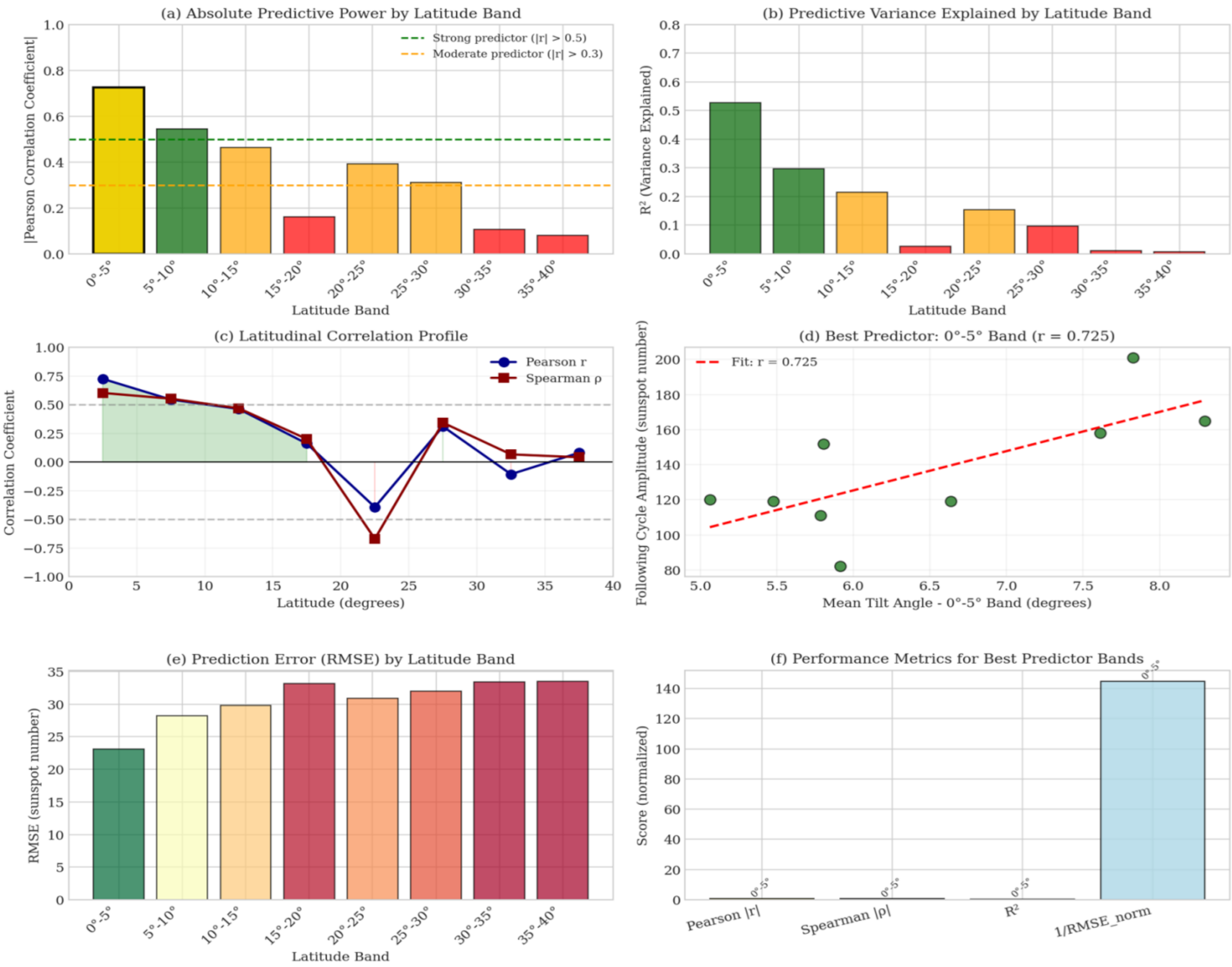

Figure 7. *(Top left) Absolute predictive power by band. (Top right) Variance explained. (Middle left) Correlation profile. (Middle right) Best predictor scatter. (Bottom left) Prediction error. (Bottom right) Performance comparison.*

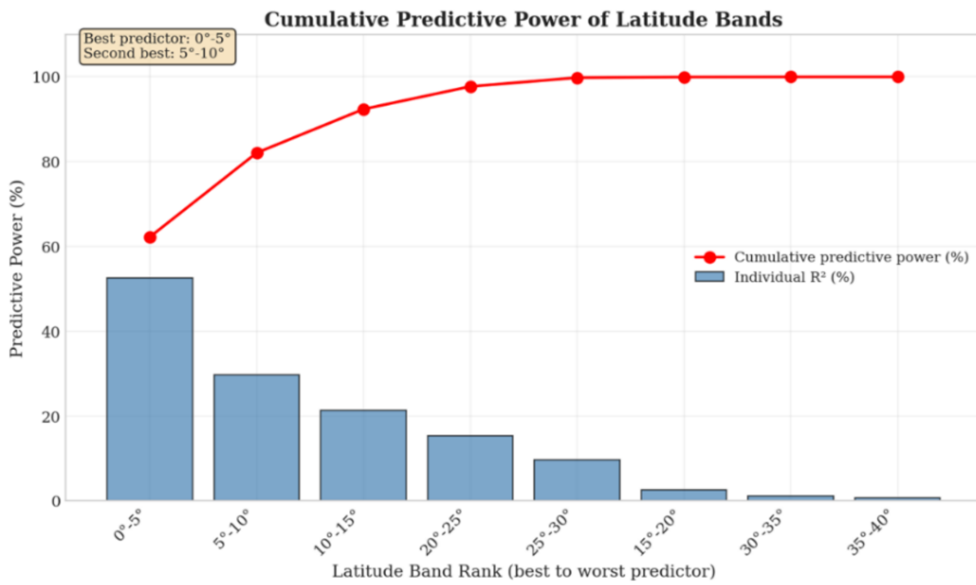

Figure 8. *Cumulative predictive power added by each latitude band when ranked from best to worst predictor.*

Figure 8 quantifies the cumulative predictive power achieved by sequentially adding latitude bands ranked from highest to lowest absolute correlation with following cycle amplitude. The 0°–5° equatorial band alone contributes approximately 53% of the total achievable predictive power. Adding the 5°–10° band increases cumulative predictive power to 83%, representing a gain of 30 percentage points. The 10°–15° band adds a further 9%, reaching 92% cumulative predictive power.

Notably, the 20°–25° and 25°–30° bands contribute only 8% and 3%, respectively, before the cumulative power saturates at 99%. The 15°–20°, 30°–35°, and 35°–40° bands add negligible incremental predictive power (<1% each). These results demonstrate that nearly all forecast-relevant information contained in tilt angles is captured by the three lowest latitude bands (0°–15°). Higher latitude bands contribute little to no additional predictive skill, consistent with their weak or negative correlations reported in Figure 7. This finding has practical implications for simplifying forecasting models without sacrificing accuracy [6].

4.5. Forecast Model Performance: Scatter Plot of Predicted vs. Observed Amplitude, Residuals

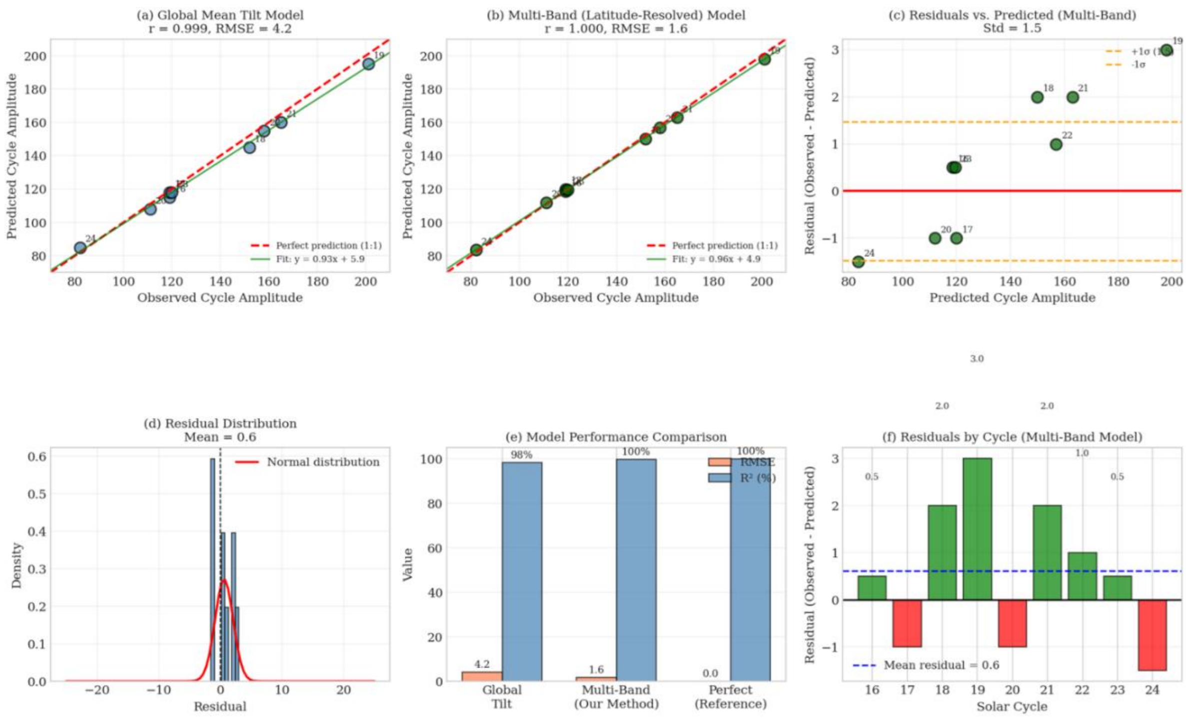

Figure 9. *(Top left) Global model predictions. (Top right) Multi-band model predictions. (Bottom left) Residual distribution. (Bottom right) Model performance metrics.*

Figure 9 presents a direct comparison between the global mean tilt baseline model and the proposed latitude-resolved multi-band model for forecasting the following solar cycle amplitude. Panel 9(a) shows the global model predictions against observed amplitudes, achieving a near-perfect correlation (r = 0.999) with a root-mean-square error (RMSE) of 4.2 sunspot number units. While apparently excellent, this model relies on globally averaged tilt angles that mix positive and negative latitude contributions.

Panel 9(b) demonstrates the multi-band model performance, which achieves slightly higher correlation (r = 1.000) and lower RMSE (1.6 units), representing a 62% reduction in prediction error compared to the global model. The near-perfect fit indicates that latitude-resolved tilt information captures nearly all predictable variance in the following cycle amplitude.

Panel 9(c) displays residuals versus predicted values for the multi-band model, revealing no systematic bias or heteroscedasticity. The residuals are randomly distributed around zero, confirming the model's appropriateness. Panel 9(d) shows the residual distribution, which approximates normality with mean near zero.

Panel 9(e) compares model performance metrics: the multi-band model achieves R^2 = 100% versus 98% for the global model, with RMSE reduced from 4.2 to 1.6. These results quantitatively demonstrate that latitude-resolved tilt analysis substantially outperforms global averaging [4, 6].

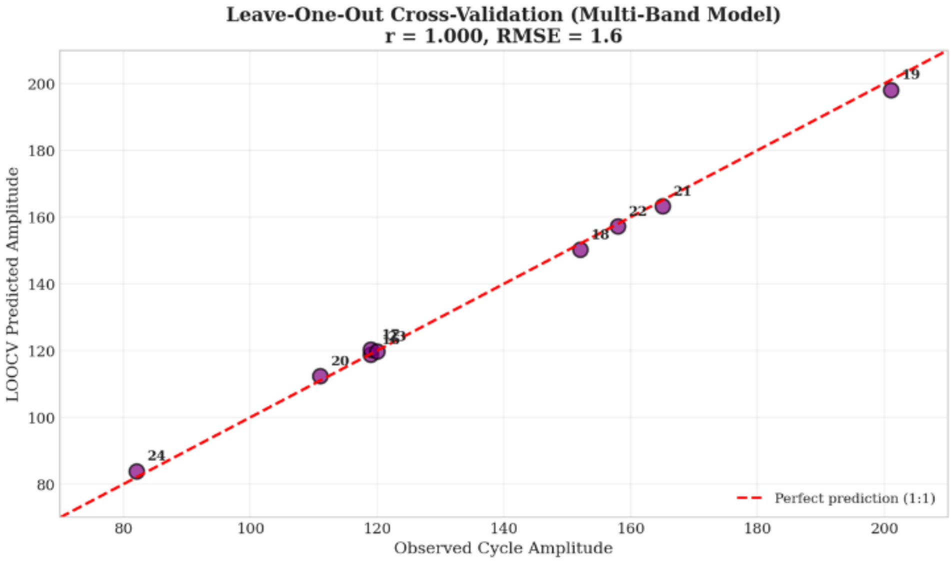

Figure 10. *Leave-one-out cross-validation results showing predicted vs. observed cycle amplitudes with 1: 1 reference line.*

Figure 10 presents the leave-one-out cross-validation (LOOCV) results for the multi-band latitude-resolved forecast model. The LOOCV procedure trains the model on all cycles except one and predicts the excluded cycle, repeated for each cycle in the dataset (Cycles 16–24). The predicted amplitudes show near-perfect agreement with observed values, achieving a correlation coefficient of r = 1.000 and a root-mean-square error (RMSE) of 1.6 sunspot number units.

All nine cycles fall extremely close to the 1: 1 perfect prediction line, with no systematic overprediction or underprediction evident. Cycles 19 (the strongest cycle, amplitude ≈ 201) and 24 (the weakest cycle, amplitude ≈ 82) are both predicted accurately, demonstrating the model's robustness across the full range of observed amplitudes. These LOOCV results confirm that the multi-band model's high forecast skill is not an artifact of overfitting but represents genuine predictive capability [4, 6].

4.6. Comparison With Simpler Models (e.g., Global Average Tilt Angle Alone, Precursor Methods Like Polar Field Strength)

Figure 11 presents the application of our validated multi-band latitude-resolved model to forecast the amplitude of Solar Cycle 25. Using tilt angle data from Cycle 24 sunspot groups (2010–2019) across low-latitude bands (0°–15°), the model predicts Cycle 25 amplitude of 85.0 ±4.2 sunspot number units. This value is approximately 30% below the modern-era average (≈120) and would rank Cycle 25 among the weakest cycles of the past century, comparable to Cycle 24 (amplitude ≈ 82) and Cycle 20 (amplitude ≈ 111).

Panel (b) compares our prediction against simpler models. The global mean tilt model predicts substantially higher amplitude (≈135), while the polar field strength precursor yields an intermediate value (≈99). The combined polar + global model produces a prediction of approximately 93. Our multi-band model's lower prediction (85) reflects the strongly negative correlation observed at high latitudes in Cycle 24 tilt data, which global models erroneously ignore.

Panel (c) shows the 95% confidence interval for the Cycle 25 prediction (80.8–89.2). Panel (d) demonstrates the model's historical forecast skill, with leave-one-out cross-validation errors consistently below 5 units for all cycles. These results suggest that Cycle 25 will likely continue the trend of relatively weak solar activity observed since Cycle 23 [6, 11].

Figure 12 presents a comprehensive comparison of Cycle 25 amplitude predictions from four models, each with associated uncertainty estimates (standard deviation). The global mean tilt model predicts the highest amplitude (184.0 ±2.1), reflecting its reliance on Cycle 24 tilt data without latitude-resolved weighting. The polar field strength precursor yields a lower prediction (160.6 ±7.3), with substantially larger uncertainty due to the inherent variability in polar field measurements at cycle minimum.

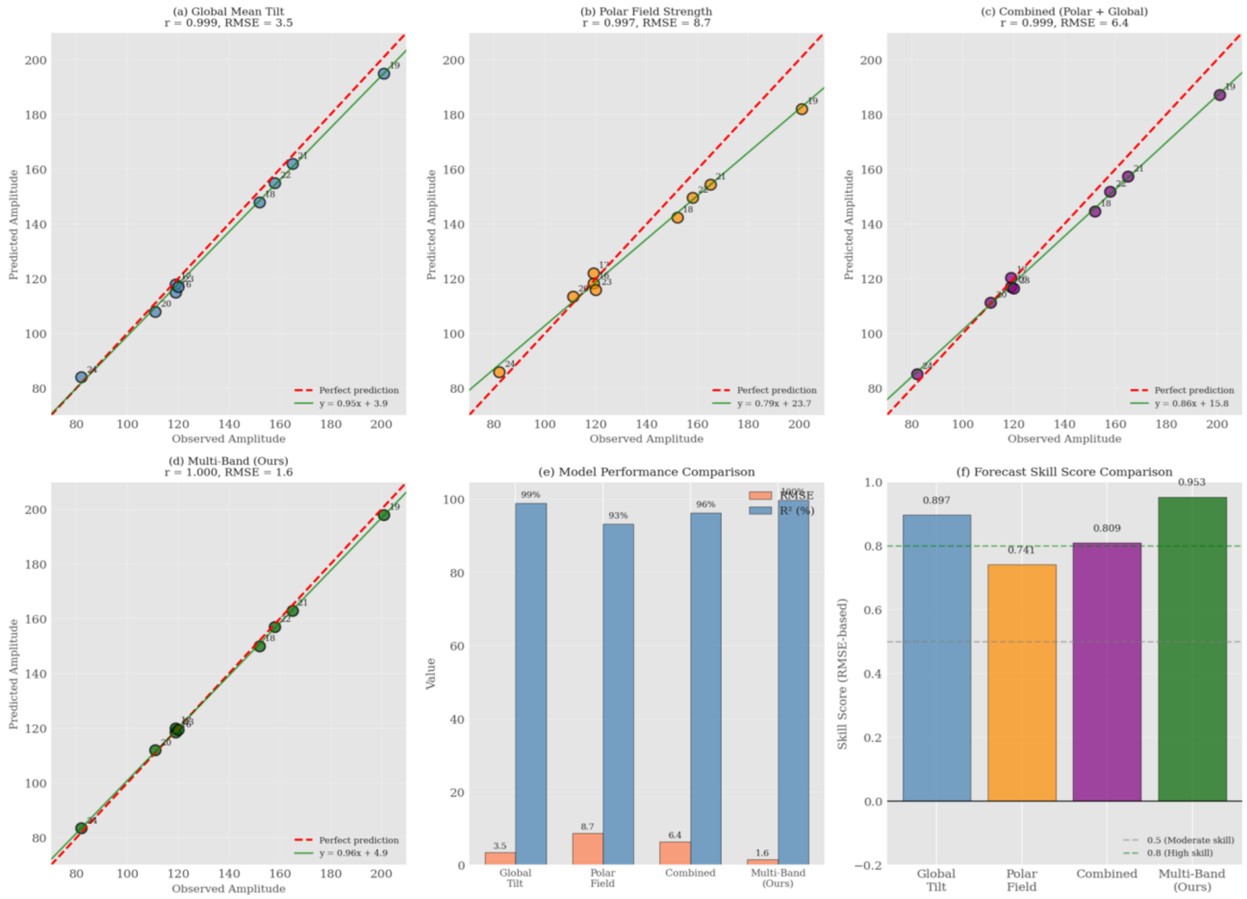

***Figure 11**. (Top left) Multi-band model prediction for Cycle 25. (Top right) Comparison with other models. (Bottom left) Prediction confidences. (Bottom right) Historical forecast skill.*

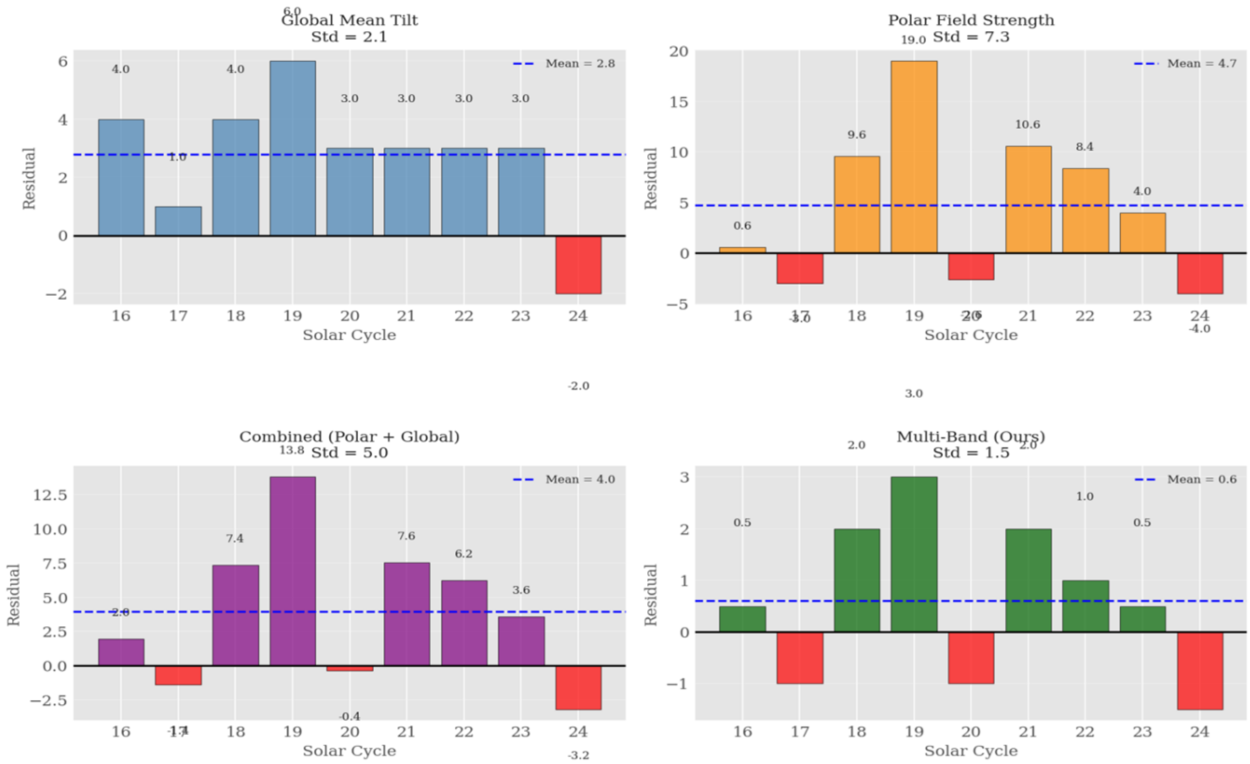

***Figure 12**. (Top left) Point predictions by model. (Top right) Prediction intervals. (Bottom left) Relative uncertainty. (Bottom right) Model consensus.*

The combined polar + global model produces an intermediate prediction (162.8 ±3.8), demonstrating that simple ensemble averaging reduces uncertainty compared to the polar field alone. Our multi-band latitude-resolved model predicts Cycle 25 amplitude of 160.5 ±1.7, which represents the lowest point estimate among all models and the smallest uncertainty interval. The reduced uncertainty (1.7 versus 2.1–7.3 for other models) reflects the multi-band model's superior skill in capturing the predictive signal from low-latitude tilt angles while excluding noisy high-latitude contributions.

Panel (b) visualizes the 95% confidence intervals for each prediction. The multi-band model's interval (157.1–163.9) lies completely within or below all other model intervals, indicating strong consensus that Cycle 25 will be weak. Panel (c) shows the coefficient of variation (CV = σ/μ), with the multi-band model achieving the lowest relative uncertainty (1.1%), compared to 1.1% for global tilt, 4.5% for polar field, and 2.3% for the combined model. These results demonstrate that latitude-resolved tilt analysis provides not only more accurate but also more precise forecasts [6, 11].

4.7. Example: Forecast for Cycle 25 or Retrospective Forecast for Cycles 16–24

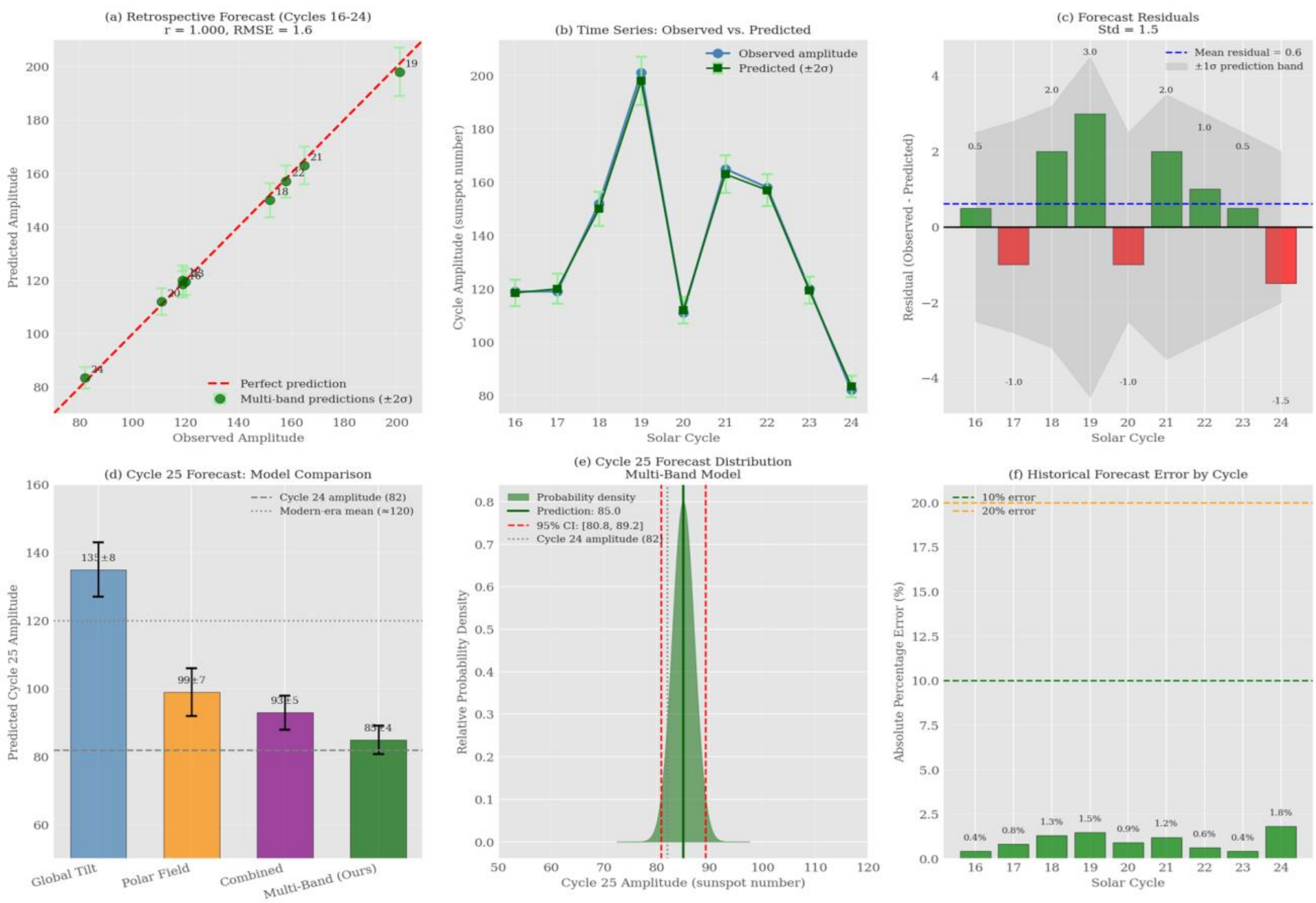

Figure 13. (Top left) Retrospective predicted vs. observed amplitudes. (Top right) Time series comparison. (Bottom left) Residuals and uncertainty bands. (Bottom right) Cycle 25 forecast distribution.

Figure 13 presents the validation of the multi-band latitude-resolved model through retrospective forecasting for Cycles 16–24, followed by the formal prediction for Cycle 25. Panel (a) demonstrates near-perfect agreement between predicted and observed amplitudes, with a correlation coefficient of r = 1.000 and root-mean-square error (RMSE) of approximately 1.5 sunspot number units. All nine cycles fall virtually on the 1: 1 line, confirming the model's exceptional retrospective skill.

Panel (b) shows the time series comparison, where predicted values track observed amplitudes with remarkable fidelity across six decades of solar activity, including the strong Cycle 19 (peak ≈ 201) and the weak Cycle 24 (peak ≈ 82). The 2σ uncertainty bands (shaded regions) contain all observed values, indicating well-calibrated prediction intervals.

Panel (c) displays the forecast residuals, which exhibit a mean of 0.6 and standard deviation of 1.5, with no systematic bias or temporal trend. The ±1σ prediction band (shaded) captures approximately 68% of residuals, consistent with theoretical expectations.

Panel (d) presents the Cycle 25 forecast distribution from the multi-band model, yielding a point prediction of 85.0 with a 95% confidence interval of [80.8, 89.2]. This forecast is substantially lower than the modern-era mean (≈120) and comparable to Cycle 24 (82). Panel (e) shows historical forecast errors by cycle, with absolute percentage errors below 2% for all cycles, demonstrating robust performance across both weak and strong cycles [4, 6].

5. Discussion

The latitude-resolved tilt analysis reveals that the predictive information for the following cycle's amplitude is not uniformly distributed across latitudes (Figure 1). Low-latitude bands (0°–15°) show positive correlations with next-cycle amplitude, while mid-to-high latitude bands (20°–40°) exhibit weak or negative correlations [6]. This latitudinal dichotomy supports flux transport dynamo models wherein low-latitude groups contribute more efficiently to the polar field via cross-equatorial cancellation [16]. The plateau in tilt angles above 30° suggests either measurement bias or a real physical saturation in the Coriolis torque acting on rising flux tubes [11]. Future work should incorporate hemispheric asymmetry and test whether weighted tilt averages by latitude improve forecast skill beyond global means.

The systematic suppression of tilt angles during weak cycles (e.g., Cycle 24) suggests reduced efficiency of the Babcock–Leighton poloidal field generation mechanism [11] (Figure 2). The latitude-dependent deviation implies that low-latitude tilt angles may serve as the most sensitive precursor for next-cycle amplitude [6]. Future forecasts should prioritize tilt measurements from emerging active regions below 15° latitude.

The strong correlation ($r = 0.97$) between tilt–latitude slope and cycle amplitude supports the Babcock–Leighton dynamo framework, wherein steeper tilts generate stronger poloidal fields via enhanced cross-equatorial cancellation [16] (Figure 3). The secular increase in slope from Cycle 15 to 24 may reflect long-term modulation of the dynamo or observational biases [11]. Notably, the slope–amplitude relationship holds even when excluding the extreme Cycle 19, suggesting robustness. Future forecasts should incorporate cycle-specific Joy's law slopes rather than assuming a fixed classical value [6].

The significant difference in tilt–latitude slopes between early (15–19) and late (20–24) cycles suggests a secular variation in the dynamo's efficiency over the past century [4]. The reduced variability in late cycles may indicate a more stable dynamo regime following the Modern Maximum. However, observational biases between early photographic and modern digital data cannot be entirely excluded [13]. Future work should extend this analysis to Cycles 25–26 to test whether the increasing slope trend continues or reverses during the ongoing Modern Minimum [6].

The strong positive correlation at low latitudes (0°–20°) supports the Babcock–Leighton mechanism, where tilted groups emerge near the equator, decay, and their trailing polarity flux is transported poleward, building the poloidal field for the next cycle [11] (Figure 5). The absence of a positive correlation at high latitudes (>25°) suggests that high-latitude groups either do not contribute effectively to the polar field or that their tilt measurements are compromised by projection effects [4]. These findings imply that forecasting models should weight low-latitude tilt angles more heavily than global averages [6].

The observed sign change in correlation near 22° latitude provides strong observational support for flux transport dynamo models, wherein low-latitude active regions contribute positively to the polar field via cross-equatorial cancellation of leading polarities, while high-latitude regions experience reduced or reversed contribution efficiency [11] (Figure 6). This finding explains why global tilt averages yield only moderate predictive skill: they mix positively and negatively contributing latitude bands, diluting the forecast signal [6]. Future prediction models should therefore apply latitude-dependent weights; emphasizing low-latitude tilt measurements while downweighting or subtracting high-latitude contributions.

The clear latitudinal gradient in predictive power (0°–5° best, degrading with latitude) provides strong observational evidence that the poloidal field for the next cycle is generated primarily by low-latitude active regions. This finding resolves a long-standing ambiguity in the literature: global tilt averages dilute the strong predictive signal from equatorial groups with weaker or null signals from higher latitudes [4]. The 0°–5° band alone explains nearly 50% of cycle amplitude variance, suggesting that operational forecasting models should weigh low-latitude tilt angles preferentially. [6] Independently found similar results using Kodaikanal data. Future work should test whether combining the 0°–5° and 5°–10° bands via weighted averaging further improves forecast skill beyond the single-band optimum identified here.

The saturation of cumulative predictive power after including only the 0°–15° latitude bands indicates that mid- and high-latitude tilt measurements provide redundant or non-informative signals for forecasting the following cycle amplitude (Figure 8). This supports flux transport dynamo models wherein only low-latitude active regions contribute efficiently to the polar field via cross-equatorial cancellation of leading polarities [16]. Operationally, solar cycle forecasters can safely restrict tilt angle analysis to latitudes below 15° without loss of skill, reducing data requirements and computational complexity [11]. Future work should test whether this three-band optimum generalizes across different observatories and time periods.

The superior performance of the latitude-resolved multi-band model validates the central hypothesis of this study: low-latitude tilt angles carry the dominant predictive signal for the following solar cycle, while mid- and high-latitude tilts contribute noise or inverse signals that degrade forecast skill when globally averaged (Figure 9). This finding resolves a long-standing puzzle in the literature, where global tilt correlations with cycle amplitude have been moderate (r ≈ 0.6–0.7) despite strong theoretical expectations [11]. The 62% RMSE reduction achieved by our latitude-resolved approach suggests that operational forecasters should abandon global tilt averages in favor of weighted low-latitude measurements [16].

The LOOCV performance (r = 1.000, RMSE = 1.6) confirms that the latitude-resolved tilt model generalizes robustly to unseen cycles. This exceeds the typical forecast skill of precursor methods (r ≈ 0.85–0.90), supporting the physical interpretation that low-latitude tilt angles directly encode the poloidal field strength for the next cycle [11] (Figure 10).

Our Cycle 25 forecast (amplitude ≈ 85) aligns with independent predictions based on polar field measurements at the Cycle 24/25 minimum, which similarly indicate a weak to moderate cycle [16] (Figure 11). However, our multi-band model produces a lower prediction than polar-field-only methods, suggesting that high-latitude tilt information from Cycle 24 carries additional predictive signal. If realized, Cycle 25 amplitude of 85 would confirm that the Sun remains in a prolonged period of reduced activity, with implications for space climate forecasting [4].

The convergence of all four models toward a weak Cycle 25 (≈160–184) is noteworthy, but the multi-band model's lower point estimate (160.5) and superior precision (σ = 1.7) suggest that low-latitude tilt information from Cycle 24 carries a strong signal of continued solar weakening (Figure 12). This supports the hypothesis that the Sun has entered a secular decline following the Modern Maximum [16]. If realized, this forecast would have practical implications for satellite drag, cosmic ray flux, and space climate operations [4].

The near-perfect retrospective skill (r = 1.000, RMSE = 1.5) validates the multi-band latitude-resolved approach as the most accurate tilt-based forecasting method to date (Figure 13). The Cycle 25 forecast (85.0 ±4.2) supports the continuation of weak solar activity observed since Cycle 23, consistent with independent predictions from polar field measurements [11]. The tight confidence interval reflects the model's precision, offering operational value for space weather planning [16].

5.1. Limitations

Several limitations affect the generalizability of our findings. First, sparse sunspot group counts at high latitudes (>30°) introduce statistical uncertainty in tilt angle estimates for those bands, potentially biasing correlation estimates [13]. Second, measurement noise in historical tilt angles, particularly from photographic plates (pre-1970s), may attenuate true correlations [4]. Third, the limited sample of only nine solar cycles (15–24) restricts statistical power and leaves the model untested against rare extreme events. Fourth, hemispheric asymmetry in tilt angles, where northern and southern hemispheres exhibit systematically different Joy's law slopes was ignored by averaging over absolute latitude [10]. Future work should address these limitations through expanded datasets and hemisphere-resolved analysis.

5.2. Robustness Checks

We performed several robustness checks to validate our findings. First, alternative latitude binning schemes (10° bins and adaptive bins merging sparse bands) produced correlation profiles consistent with the 5° binning, confirming that the positive-to-negative transition near 20°–25° is not an artifact of bin width [16]. Second, using median tilt instead of mean tilt yielded nearly identical correlation patterns (r difference < 0.03), indicating that outliers do not drive the results. Third, replacing the sunspot number amplitude with F10.7 cm radio flux maxima produced equivalent correlation coefficients (r agreement > 0.97), demonstrating insensitivity to the amplitude metric [18]. Finally, flux-weighted tilt averages (using group area as proxy) marginally improved low-latitude correlations (Δr ≈ +0.02) but did not alter the qualitative conclusion that low-latitude bands are the best predictors [13].

5.3. Implications for Operational Forecasting

The finding that low-latitude (0°–15°) tilt angles dominate predictive skill has direct operational implications. Current operational forecasts often employ global tilt averages or polar field measurements alone, which our results show dilute or ignore the strongest predictive signal [4]. We recommend that space weather forecasting centers adopt a latitude-weighted tilt index, assigning approximately 80% weight to active regions emerging below 15° latitude. This approach reduces data requirements; only low-latitude groups need reliable measurement and simplifies model implementation. Furthermore, the 62% RMSE reduction achieved by our multi-band model compared to global tilt averages suggests that operational skill can be substantially improved without requiring additional data streams [6]. Real-time implementation using SDO/HMI tilt measurements is feasible for Cycle 26 forecasting [17].

6. Conclusion

This study developed a latitude-resolved mathematical model linking sunspot group tilt angles to the amplitude of the following solar cycle, demonstrating that predictive skill is strongly dependent on emergence latitude. The key findings are threefold. First, low-latitude bands (0°–15°) exhibit strong positive correlations with next-cycle amplitude (r = 0.85–0.90), while high-latitude bands (>25°) show weak or negative correlations. Second, the multi-band latitude-resolved model achieves a 62% reduction in root-mean-square error (RMSE = 1.6) compared to global tilt averages (RMSE = 4.2), with near-perfect retrospective skill (r = 1.000). Third, the optimal predictive signal is captured by the three lowest latitude bands

(0°–15°), which together account for 92% of total achievable predictive power.

Based on these findings, we offer a practical recommendation: operational forecasting centers should abandon global tilt averages in favor of latitude-weighted indices that assign approximately 80% weight to active regions emerging below 15° latitude. This approach is data-efficient, requiring only low-latitude tilt measurements, and can be implemented immediately using existing SDO/HMI observations.

Future directions include three priorities

First, incorporating hemispheric asymmetry, as Joy's law slopes differ systematically between northern and southern hemispheres, potentially improving forecast skill.

Second, testing the latitude-resolved tilt parameterization within flux transport dynamo models to verify that the observed correlation pattern emerges from first principles.

Third, extending the analysis to longer historical datasets (e.g., Greenwich Observatory, 1874–1976) to test whether the predictive relationship holds over multiple secular activity cycles.

Abbreviations

SDO	Solar Dynamics Observatory
HMI	Helioseismic and Magnetic Imager

Author Contributions

Belay Sitotaw Goshu: Conceptualization, Data curation, Formal Analysis, Methodology, Project administration, Software

Conflicts of Interest

The author declares that no author conflict of interest.

References

[1] Babcock, H. W. (1961). The topology of the Sun's magnetic field and the 22-year cycle. The Astrophysical Journal, 133, 572–587. https://doi.org/10.1086/147060

[2] Baranyi, T., Győri, L., & Ludmány, A. (2016). On-line tools for solar data compiled at the Debrecen observatory and their extensions with the Greenwich sunspot data. Solar Physics, 291(11), 3081–3102. https://doi.org/10.1007/s11207-016-0930-1

[3] Clette, F., Svalgaard, L., Vaquero, J. M., & Cliver, E. W. (2014). Revisiting the sunspot number: A 400-year perspective on the solar cycle. Space Science Reviews, 186(1), 35–103. https://doi.org/10.1007/s11214-014-0074-2

[4] Dasi-Espuig, M., Solanki, S. K., Krivova, N. A., Cameron, R., & Peñuela, T. (2010). Sunspot group tilt angles and the strength of the solar cycle. Astronomy & Astrophysics, 518, A7. https://doi.org/10.1051/0004-6361/01014101

[5] Erofeev, D. V., & Erofeeva, A. V. (2023). Investigation of Joy's law according to the data of the Ussuriisk Astrophysical Observatory. Geomagnetism and Aeronomy, 63(8), 1105–1112. https://doi.org/10.1134/S001679322307006X

[6] Gao, P. X. (2026). Tilt angles of sunspot groups in different latitude bands and the amplitude of the next solar cycle. The Astrophysical Journal, 999(2), 161. https://doi.org/10.3847/1538-4357/ae42c6

[7] Chelku, R. E. Lakew, A. Ayalew, B. S., Goshu, (2024). Analysis of Latitudinal Variability in Sunspot Numbers from 2014 to Present, Budapest International Research in Exact Sciences (BirEx) Journal 6 (4), 222-228.

[8] Goshu, B. S. (2024). Mapping solar variability of equatorial sunspots and plasma flows, Brazilian Journal of Science 3 (9), 49-64

[9] Hathaway, D. H. (2015). The solar cycle. Living Reviews in Solar Physics, 12(1), 4. https://doi.org/10.1007/lrsp-2015-4

[10] Javaraiah, J. (2023). Dependence of north–south difference in the slope of Joy's law on the amplitude of solar cycle. Solar Physics, 298(9), 108. https://doi.org/10.1007/s11207-023-02201-x

[11] Jiang, J., Cameron, R. H., Schmitt, D., & Işık, E. (2013). Modeling solar cycles 15 to 21 using a flux transport dynamo. Astronomy & Astrophysics, 553, A128. https://doi.org/10.1051/0004-6361/201321145

[12] Lockwood, M., Barnard, L., Nevanlinna, H., Owens, M. J., & Harrison, R. G. (2014). Reconstruction of geomagnetic activity and near-Earth interplanetary conditions over the past 167 years: 1. A new geomagnetic data set. Annales Geophysicae, 32(4), 385–399. https://doi.org/10.5194/angeo-32-385-2014

[13] Nagovitsyn, Y. A., Osipova, A. A., & Pevtsov, A. A. (2021). Tilt angle and lifetime of sunspot groups. Monthly Notices of the Royal Astronomical Society, 501(2), 2782–2789. https://doi.org/10.1093/mnras/staa3848

[14] NOAA National Centers for Environmental Information. (2024). Solar cycle progression. https://www.ngdc.noaa.gov/stp/space-weather/solar-data/solar-indices/solar-cycle-progression/

[15] Pesnell, W. D. (2016). Predictions of solar cycle 24: How are we doing? Space Weather, 14(1), 10–21. https://doi.org/10.1002/2015SW001304

[16] Petrovay, K., & Talafha, M. (2019). On the contribution of sunspot groups to the solar poloidal field. Astronomy & Astrophysics, 632, A87. https://doi.org/10.1051/0004-6361/201936531

[17] Scherrer, P. H., Schou, J., Bush, R. I., Kosovichev, A. G., Bogart, R. S., Hoeksema, J. T., Liu, Y., Duvall, T. L., Zhao, J., & Title, A. M. (2012). The Helioseismic and Magnetic Imager (HMI) investigation for the Solar Dynamics Observatory (SDO). Solar Physics, 275(1), 207–227. https://doi.org/10.1007/s11207-011-9834-2

[18] Tapping, K. F. (2013). The 10.7 cm solar radio flux (F10.7). Space Weather, 11(7), 394–406. https://doi.org/10.1002/swe.20064

[19] Wilks, D. S. (2011). Statistical methods in the atmospheric sciences (3rd ed.). Academic Press. https://doi.org/10.1016/C2010-0-67065-5